Available online at www.sciencedirect.com
ScienceDirect
Materials Science and Engineering C 28 (2008) 421–428
MATERIALS SCIENCE & ENGINEERING C
www.elsevier.com/locate/msec

A scalable model for trilayer conjugated polymer actuators and its experimental validation

Yang Fang [a], Xiaobo Tan [a,*], Yantao Shen [a], Ning Xi [a], Gursel Alici [b]

[a] Department of Electrical and Computer Engineering, Michigan State University, East Lansing, MI 48824, USA
[b] School of Mechanical, Materials and Mechatronics Engineering, University of Wollongong, 2522 NSW, Australia

Available online 14 April 2007

Abstract

Conjugated polymers are promising actuation materials for bio/micromanipulation systems, biomimetic robots, and biomedical devices. For these applications, it is highly desirable to have predictive models available for feasibility study and design optimization. In this paper a scalable model is presented for trilayer conjugated polymer actuators based on J. Madden's diffusive-elastic-metal model. The proposed model characterizes actuation behaviors in terms of intrinsic material parameters and actuator dimensions. Experiments are conducted on polypyrrole actuators of different dimensions to validate the developed scaling laws for quasi-static force and displacement output, electrical admittance, and dynamic displacement response.

Keywords: Conjugated polymer actuators; Artificial muscles; Polypyrrole (PPy); Scalable model; Experimental validation

1. Introduction

Electroactive polymers (EAPs), also known as artificial muscles, are emerging actuation and sensing materials with numerous potential applications in biomimetic robotics and biomedical systems [1–4]. One class of EAP materials is conjugated polymers, which are also called conducting polymers or synthetic metals [2,5]. Polypyrrole (PPy) and polyaniline are two of the most commonly used conjugated polymers for actuation purposes. The backbones of conjugated polymers have alternating single and double carbon–carbon bonds (conjugation), which results in positive charge carriers when electrons are removed from the polymers electrochemically under a sufficiently positive potential (oxidation). For a conjugated polymer in contact with an electrolyte, the oxidation process will drive anions into and/or cations out of the polymer matrix depending on the sizes of ions, to maintain the charge neutrality. Application of a sufficiently negative potential can reverse the process and *reduce* the polymer. The mass transport induced by ion movement during reduction/oxidation (redox) is considered to be the primary mechanism responsible for volumetric change and thus the actuation of conjugated polymers. An anion-transporting conjugate polymer will expand during oxidation and contract during reduction, while a cation-transporting polymer will demonstrate the opposite behavior. Conjugate polymer actuators of different configurations have been reported, e.g., bilayer benders [2], trilayer benders [6,7], and linear extenders [5,8].

Conjugated polymer actuators require low actuation voltage (under 1 V), generate considerable stress and large strain output, and are light and biocompatible. These advantages make them attractive for a wide range of robotic and biomedical applications, such as micro and biomanipulation, biomimetic systems, and biomedical devices [2,9–11]. For all these applications, from the micro scale to the macro scale, it is highly desirable to have quantitative models available that can predict quasi-static and dynamic actuation performance in terms of intrinsic material parameters and actuator dimensions. Such models will be useful in feasibility analysis, design optimization, and even actuator control. Alici and coworkers investigated modeling and geometry optimization of bending curvature and force output for trilayer PPy actuators [6,12,13]. Christophersen et al. characterized and modeled the bending curvature for bilayer PPy microactuators of different

* Corresponding author. Tel.: +1 517 4325671; fax: +1 517 3531980.
E-mail addresses: fangyang@egr.msu.edu (Y. Fang), xbtan@msu.edu (X. Tan), shenya@egr.msu.edu (Y. Shen), xin@egr.msu.edu (N. Xi), gursel@uow.edu.au (G. Alici).

0928-4931/$ - see front matter © 2007 Elsevier B.V. All rights reserved.
doi:10.1016/j.msec.2007.04.024

dimensions [14]. All these studies were focused on quasi-static operating conditions, where the bending curvature and/or force output were examined in terms of material stiffness and actuator geometry.

In this paper a scalable electrochemomechanical model is presented for trilayer conjugated polymer actuators, which can be used to predict both quasi-static and dynamic actuation performance under a given voltage input. The model consists of three modules: 1) electrochemical dynamics module, adapted from the diffusive-elastic-metal model of Madden [15]; 2) stress-generation module relating transferred charges to internal actuation stress; and 3) mechanical dynamics module. Scaling laws for key parameters of the electrical admittance model are developed, rendering the complete model expressible in intrinsic material parameters and actuator dimensions. Experiments are conducted on anion-transporting trilayer PPy actuators of different dimensions to validate the model scalability. Experimental results are presented for joint quasi-static force/bending output, admittance spectrum, and dynamic bending responses.

The remainder of the paper is organized as follows. In Section 2 the electrochemomechanical model is presented together with relevant scaling laws. In Section 3 experimental methods are described. Results and discussions are given in Section 4. Finally concluding remarks are provided in Section 5.

2. Model

The trilayer PPy actuator is illustrated in Fig. 1. In the middle is an amorphous, porous polyvinylidene fluoride (PVDF) layer that serves both as a backing material and a storage tank for the electrolyte. On both sides of the actuator are the PPy layers. When a voltage is applied across the actuator, the PPy on the anode side is oxidized while that on the cathode side is reduced. The oxidized layer absorbs anions and expands, while the reduced layer gives up anions and contracts. The differential expansion thus leads to bending of the actuator, as shown in Fig. 1 (right).

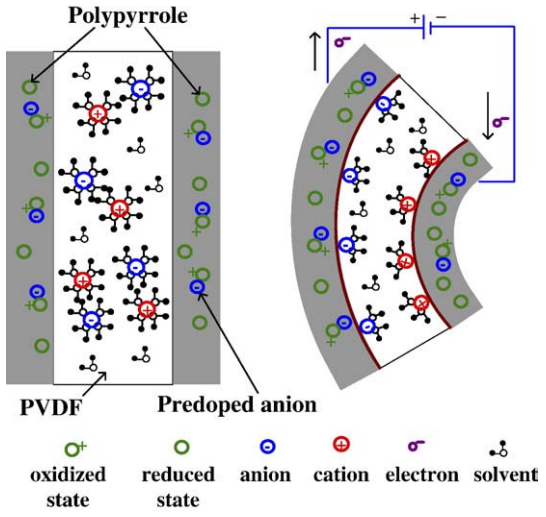

Fig. 1. Illustration of the actuation mechanism of trilayer polypyrrole actuator. Left: the sectional view of the trilayer structure; right: bending upon application of a voltage.

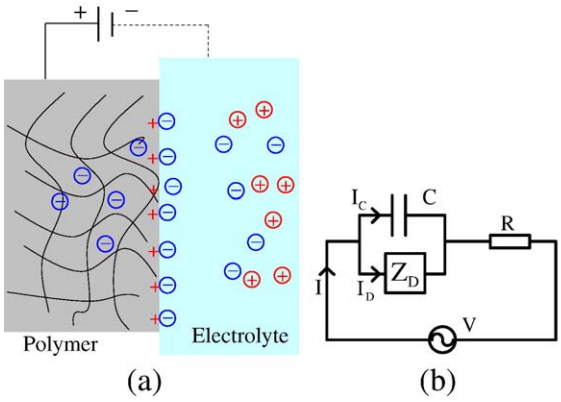

Fig. 2. (a) Illustration of double-layer charging and diffusion for a conjugated polymer film with one side in contact with electrolyte (representing half of the trilayer actuator); (b) equivalent circuit model for the polymer impedance.

2.1. Electrochemomechanical model

The electrochemomechanical model consists of three modules: 1) the electrical admittance module relating the current (and thus the charge transferred) to the voltage input; 2) the electromechanical coupling module expressing the generated stress in terms of the transferred charge; and 3) the mechanical module connecting the stress to the displacement or force output.

2.1.1. Electrical admittance module

The voltage input of the actuator is applied across the two PPy layers. This produces a potential difference between each PPy layer and the electrolyte, as illustrated in Fig. 2(a). Note that only one side of the PPy is in contact with the electrolyte. Under the potential difference, the anions in the electrolyte migrate toward the polymer, which results in double-layer charges at the polymer/electrolyte interface — like a double-layer capacitance with an equivalent thickness of δ. There are two possible mechanisms for the accumulated anions to enter the polymer matrix, diffusion and migration. However, it was shown that the migration effect is negligible when the polymer is highly conductive [16]. Madden thus proposed a diffusive-elastic-metal model for PPy, where it was assumed that the polymer matrix is perfectly conducting and the ion transport within the polymer is solely determined by diffusion [15]. The admittance model showed good agreement with experimental data for a wide frequency range from 10^{-4} to 10^{5} Hz [15], and thus will be adapted for use in this paper. Model adaptation is entailed by the different boundary conditions of the trilayer actuator from those in [15]: while ions diffuse across both polymer–electrolyte interfaces for a polymer immersed in the electrolyte [15], ion diffusion takes place only through the PPy–PVDF interface and there is no ion flux on the PPy–air interface for the trilayer actuator. Fig. 2(b) shows an equivalent circuit model of the polymer impedance, where the faradaic current has been ignored. C denotes the double-layer capacitance at the

polymer/electrolyte interface, R is the electrolyte and contact resistance, and Z_D represents the "diffusion impedance". The admittance $Y(s)$ of the trilayer actuator can be derived [17]:

$$Y(s)=\frac{I(s)}{V(s)}=\frac{s\left[\frac{\sqrt{D}}{\delta}\tanh\left(h\sqrt{s/D}\right)+\sqrt{s}\right]}{2\left(\frac{\sqrt{s}}{C}+Rs^{3/2}+\frac{R\sqrt{D}}{\delta}s\tanh\left(h\sqrt{s/D}\right)\right)}, \quad (1)$$

where s is the Laplace variable, h is the thickness of each PPy layer, and D is the diffusion coefficient.

2.1.2. Electromechanical coupling

The anions transferred to the polymer cause expansion of the polymer. It was shown that the induced in-plane strain is proportional to the density ρ of the transferred charges [18]: $\varepsilon=\theta\rho$, where θ is the strain-to-charge ratio. Equivalently, the induced stress by the transferred charges is

$$\sigma=\theta E_{\text{ppy}}\rho, \quad (2)$$

where E_{ppy} denotes the Young's modulus of the Ppy layer. Since the bulk capacitance of the polymer is much larger than the double-layer capacitance, the charges stored in the double layer at the steady state are negligible comparing with that in the bulk [19]. Consequently one can obtain the density $\rho(s)$ by

$$\rho(s)=\frac{I(s)}{sWLh}, \quad (3)$$

where W, L are the width and length of the Ppy.

2.1.3. Mechanical output

Consider a trilayer actuator clamped at one end, as shown in Fig. 3. Under quasi-static conditions, it can be shown through moment balance that the beam tip displacement y under the actuation-induced stress (2) and the external force F is [19]

$$F=-\gamma_1 y+\gamma_2\rho, \quad (4)$$

where the constants γ_1 and γ_2 are defined by

$$\gamma_1=\frac{4WE_{\text{ppy}}h_{\text{pvdf}}^3}{3L_f^3}\left[\left(1+\frac{h}{h_{\text{pvdf}}}\right)^3-1+\frac{E_{\text{pvdf}}}{E_{\text{ppy}}}\right],$$

$$\gamma_2=\frac{E_{\text{ppy}}\theta Wh_{\text{pvdf}}^2}{L_f}\left[\left(1+\frac{h}{h_{\text{pvdf}}}\right)^2-1\right],$$

and E_{pvdf} denotes the Young's modulus of the PVDF layer. Note that Eq. (4) characterizes the quasi-static force versus displacement relationship for a given (constant) actuation voltage through Eqs. (1) and (3).

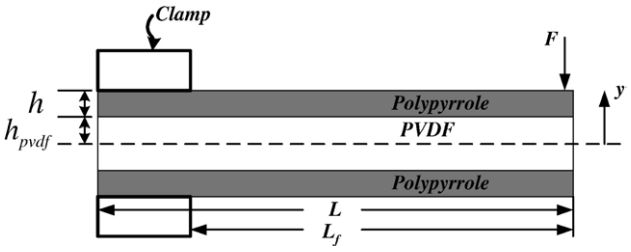

Fig. 3. Geometry of the trilayer actuator.

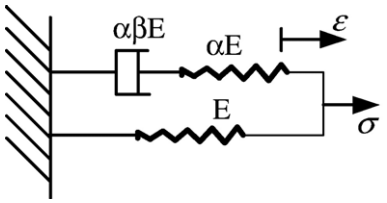

Fig. 4. Standard linear solid model for capturing polymer viscoelasticity.

When the quasi-static condition does not hold, one needs to consider the mechanical dynamics of the trilayer beam. The actuation bandwidth of a PPy actuator is typically much lower than its mechanical natural frequencies. For example, a sample of dimensions $20\times5\times0.17$ mm was measured to have an actuation bandwidth of 0.5 Hz while its natural frequency was measured to be 65 Hz. Thus the inertial dynamics will be ignored.[1] Therefore, only the material damping effect is considered in this work. The standard linear solid model, illustrated in Fig. 4, can capture the viscoelasticity of solid polymer [20], and is adopted for modeling the dynamic moduli of PVDF and PPy.

The equivalent modulus E' in Fig. 4 is

$$E'(s)=E\frac{\alpha\beta+\beta}{\beta}\cdot\frac{s+\frac{1}{\alpha\beta+\beta}}{s+\frac{1}{\beta}}. \quad (5)$$

When $F=0$ in Eq. (4), the free-bending response is obtained by combining Eqs. (1), (3), and (4):

$$\frac{y(s)}{V(s)}=\gamma_m(s)\frac{\frac{\sqrt{D}}{\delta}\tanh\left(h\sqrt{\frac{s}{D}}\right)+\sqrt{s}}{\frac{\sqrt{s}}{C}+Rs^{3/2}+R\frac{\sqrt{D}}{\delta}s\tanh\left(h\sqrt{\frac{s}{D}}\right)}, \quad (6)$$

where $\gamma_m(s)$ is defined as

$$\gamma_m(s)=\frac{3\alpha L_f^2\left[\left(1+\frac{h}{h_{\text{pvdf}}}\right)^2-1\right]}{8h_{\text{pvdf}}hWL\left[\left(1+\frac{h}{h_{\text{pvdf}}}\right)^3+\frac{E'_{\text{pvdf}}(s)}{E'_{\text{ppy}}(s)}-1\right]},$$

and $E'_{\text{pvdf}}(s)$ ($E'_{\text{ppy}}(s)$, resp.) is related to E_{pvdf} (E_{ppy}, resp.) through Eq. (5) with appropriate coefficients.

2.2. Scaling laws for double-layer capacitance and circuit resistance

Two key parameters in the electrical admittance model (1) (and thus in the force or displacement response model) are the double-layer capacitance C and the resistance R. It is of interest to know how they scale with the actuator dimensions. From the analogy to parallel-plate capacitors, one expects C to be

[1] Actuators with higher bandwidth have been recently reported [7], and one will need to include inertial dynamics for those cases.

proportional to the interface area between the PPy and the electrolyte, i.e.,

$$C = C_0 WL, \tag{7}$$

where C_0 is the double-layer capacitance per unit area.

The scaling of R is more involved. A transmission line model is proposed considering the nonzero (although low) resistivity of PPy, as shown in Fig. 5. Here the top and bottom layers represent PPy resistance while the middle layer represents the electrolyte resistance. Let r_1 and r_2 denote the resistivity of the PPy and of the electrolyte, respectively. Then the resistances R_1 and R_2 per unit distance are:

$$R1 = \frac{r_1}{hW}, R_2 = \frac{2r_2 h_{\text{pvdf}}}{W}.$$

From the basic transmission line theory [21],

$$R = \frac{\sqrt{\frac{4r_1 r_2 h_{\text{pvdf}}}{hW^2}}}{\tanh\left(L\sqrt{\frac{4r_1 r_2 h_{\text{pvdf}}}{hW^2}}\right)}, \tag{8}$$

which is expressed in terms of fundamental material parameters and layer dimensions.

The scaling laws (7) and (8) can then be plugged into Eqs. (1) and (6) to obtain scalable models for the admittance and the bending dynamics of trilayer actuators.

3. Experiment

3.1. Materials

The trilayer PPy actuator is fabricated by the Intelligent Polymer Research Institute at the University of Wollongong, Australia, and a description of the fabrication process can be found in, e.g., [7]. The PVDF layer is 110 μm thick, while each PPy layer is 30 μm thick. The electrolyte used is 0.05 M tetrabutylammonium hexafluorophosphate (TBA^+ PF_6^-) in the solvent propylene carbonate (PC). Actuators of different dimensions (length and width) are cut from the fabricated sheet. Each actuator is soaked in the electrolyte before testing for 2 h. The electrolyte stored in the PVDF layer enables the actuator to work in air for several hours.

3.2. Electrical measurement

A computer equipped with a DS1104 R&D Controller Board (dSPACE Inc) is used for data acquisition and processing. A

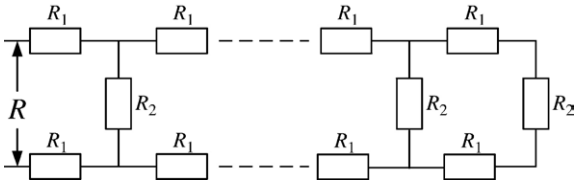

Fig. 5. The transmission line model for the circuit resistance.

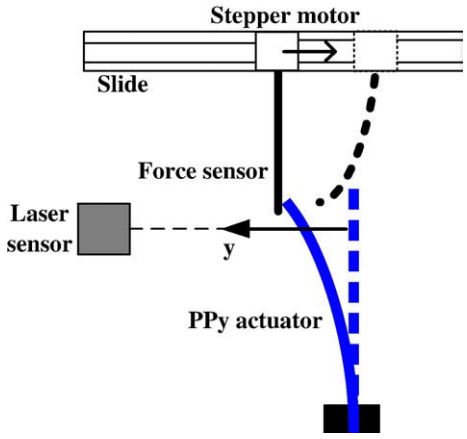

Fig. 6. Schematic of the experimental setup for joint force–displacement measurement.

trilayer actuator is clamped on one end, where electrical contacts are made using copper tapes. The applied actuation voltage and the corresponding current are measured.

To measure the double-layer capacitance C, a step voltage U of 0.4 V is applied. The transferred charge Q into the PPy layer is computed by integrating the charging current, which is obtained by subtracting the faradaic current from the total current. At the steady state, the charging dynamics dies out and a very small DC current (typically below 0.05 mA for the experiments conducted) is observed, which is taken to be the faradaic current. It can be shown from Eq. (1) (using the Final Value Theorem [22]) that

$$Q = \frac{1}{2}U\left(1 + \frac{h}{\delta}\right)C, \tag{9}$$

and thus C is computed by

$$C = \frac{2Q}{U\left(1 + \frac{h}{\delta}\right)}. \tag{10}$$

The double-layer thickness δ is hard to measure directly and an estimate of 25 nm is used based on the range reported in [23].

To measure the resistance R, a high-frequency sinusoidal input $U\sin(\omega t)$ is applied. From Eq. (1), the admittance $Y(j\omega) \to \frac{1}{2R}$ as $\omega \to \infty$, i.e., the polymer becomes resistive for high-frequency inputs. Thus R is obtained from $R = \frac{1}{2|Y(j\omega)|}$. In experiments an input of frequency 250 Hz and amplitude 0.2 V is used.

In the measurement of electrical admittance spectrum, the computer generates a sequence of actuation signals with the amplitude of 0.2 V and different frequencies, from 20 Hz down to 0.05 Hz, which covers the frequency range relevant to the actuation application of the trilayer actuator.[2] The current is measured and the magnitude and phase of its fundamental-frequency component are extracted with fast Fourier transform. The admittance (magnitude and phase) at each frequency is then computed.

[2] One could also use electrical impedance spectroscopy for measurement for a wider frequency range.

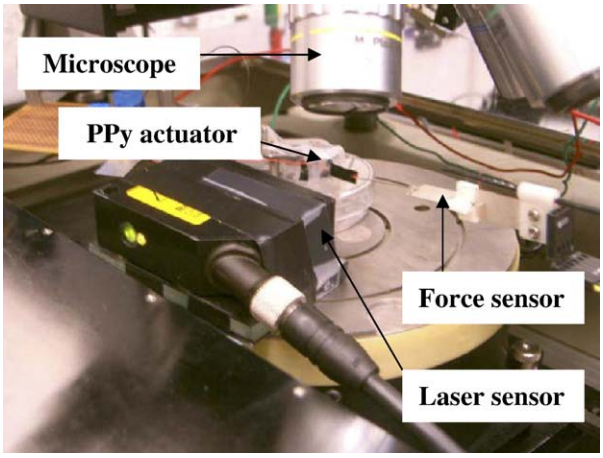

Fig. 7. The setup for force/displacement measurement.

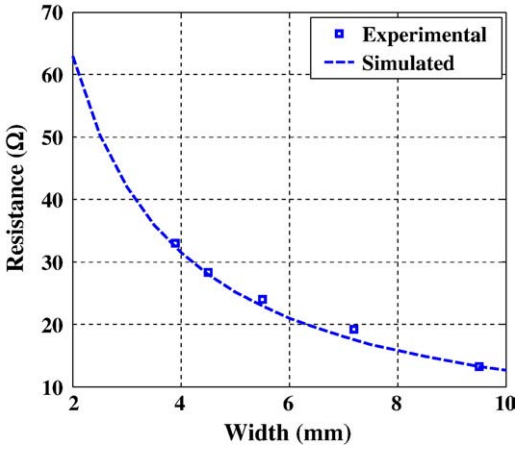

Fig. 9. Resistance versus actuator length (width=20 mm).

3.3. Force and bending measurement

A laser distance sensor (OADM 20I6441/S14F, Baumer Electric) with resolution of 5 μm is used to measure the bending displacement of the actuator. Quasi-static force/displacement measurement is conducted using an experimental setup illustrated in Fig. 6. Through the slide, a PVDF micro-force sensor [24] can measure the actuation force at different deflection levels under a given actuation voltage, from the free-bending configuration $F=0$ to the fully-blocked configuration ($y=0$). A picture of the actual setup is shown in Fig. 7.

4. Results and discussion

4.1. Verification of scaling laws for double-layer capacitance and circuit resistance

Fig. 8 shows the comparison between the measured double-layer capacitance and the predicted value from Eq. (7) for different actuator sizes ($L\times W$), where C_0 is identified to be 7.86×10^{-7} F/mm^2.

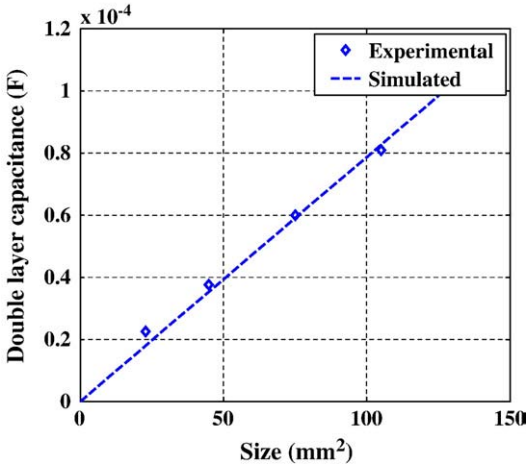

Fig. 8. Double-layer capacitance versus actuator size.

Fig. 9 compares the measured resistance R and the predicted value from Eq. (8) as a function of actuator width, while the length of actuators is fixed to 20 mm. The resistivity values of $r_1=9\times10^{-5}$ Ω m and $r_2=2.7$ Ω m are obtained by fitting the experimental data points in Fig. 9, where r_1 is restricted within the typical range [25] during tuning. As an independent validation step, the identified r_1 and r_2 are further used to predict the resistance for five 3 mm-wide actuators with different lengths.

As shown in Fig. 10, the comparison between the measured resistances and their theoretical values based on Eq. (8) confirms the prediction capability of the scaling law.

The agreement between measurement and simulation in Figs. 8–10 validates the proposed scaling laws for C and R, which will be used in the prediction of quasi-static force/displacement, electrical admittance, and dynamic displacement response in the following subsections.

4.2. Quasi-static force versus displacement output

Two sets of PPy actuators are used with widths of 3.5 and 6 mm respectively. In each set there are three samples with lengths of 20, 30 and 40 mm. Throughout the paper, the length of clamped portion $L-L_f=5$ mm. Given a constant voltage input, the current

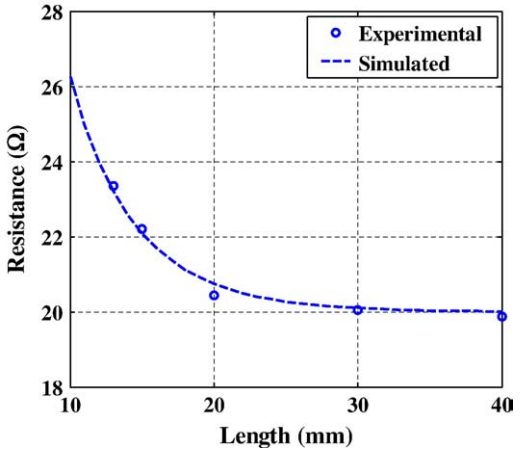

Fig. 10. Resistance versus actuator length (width=3 mm).

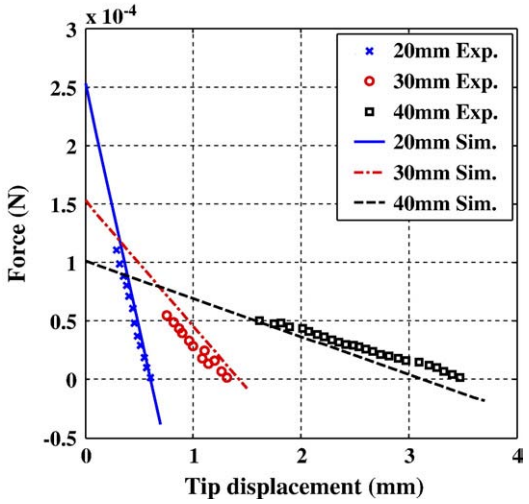

Fig. 11. Force versus displacement under an actuation voltage of 0.4 V (width=3.5 mm).

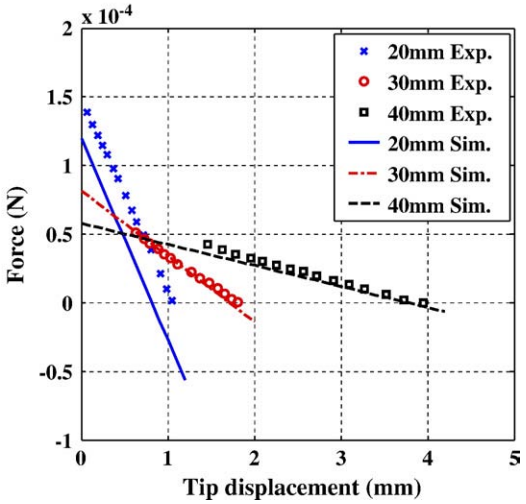

Fig. 13. Electrical admittance spectrum (size: 30×5 mm).

can be predicted by Eq. (1). Then the charge density ρ can be calculated based on Eq. (3). Thus the force versus displacement curve can be computed using Eq. (4), where E_{ppy}=80 MPa, E_{pvdf}=440 MPa [13], $\theta=1.3\times10^{-10}$ m^3 C^{-1} [15]. Fig. 11 shows the comparison between the measured force–displacement curve and the model prediction for the set of actuators with width 3.5 mm under an actuation voltage of 0.4 V. Fig. 12 shows the results for the set of actuators with width 6 mm. It can be seen that in both figures reasonable agreement between measurement and simulation is achieved. Experiments are also conducted for other actuation voltages with satisfactory agreement with model prediction. Those results will not be presented here due to space limitation. One of the implications of the results in Figs. 11 and 12 is that the longer is the actuator, the smaller is the force output, and vice versa. This fact is in agreement with the results presented in [13].

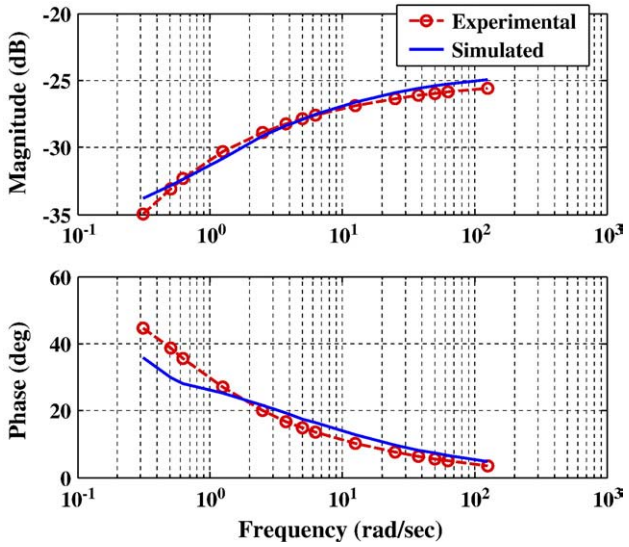

Fig. 12. Force versus displacement under an actuation voltage of 0.4 V (width=6 mm).

4.3. Electrical admittance spectrum

In Fig. 13 the measured admittance is compared to the predicted one for an actuator of size 30×5 mm, while in Fig. 14 the same is presented for an actuator of size 40×5 mm. In both figures the agreement in magnitude plots is excellent. In the mean time the match for the phase plots is good except for the relatively big discrepancy at the low-frequency end. The low-frequency phase mismatch is likely due to the change of actuation behavior in air when the solvent evaporates over time (the high-frequency measurements are done in a short period of time and the behavior change there is minimal).

4.4. Dynamic displacement response

Finally the model (6) for the dynamic displacement response is examined for a range of actuation frequencies for two different actuator sizes, 30×5 mm and 40×5 mm. The comparison

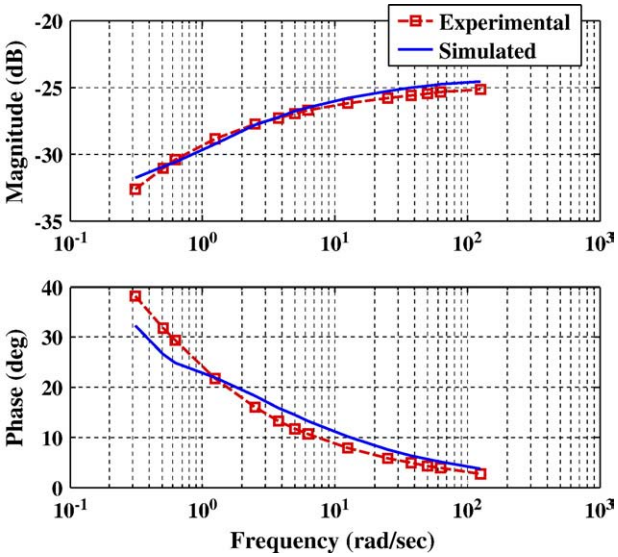

Fig. 14. Electrical admittance spectrum (size: 40×5 mm).

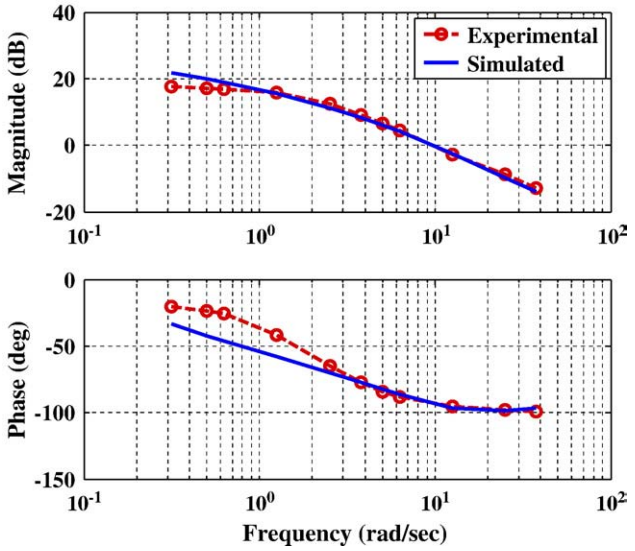

Fig. 15. Dynamic displacement response (size: 30×5 mm).

between the experimental measurement and the model prediction is shown in Figs. 15 and 16. The coefficients related to dynamic modulus in Eq. (5) for PPy and PVDF are identified based on curve fitting: $\alpha=5.02$ and $\beta=0.83$ for PPy, and $\alpha=4.68$ and $\beta=0.044$ for PVDF. From the figures the agreement between measurement and simulation is good for the magnitude plots. However, mismatch exists in the low-frequency portion of the phase plots. The cause of this, other than the possible behavior change due to solvent evaporation, is currently under investigation.

4.5. Influence of PPy redox level on material properties

In general the redox level of a conjugated polymer could affect its conductivity and Young's modulus [26]. In the development of the scalable model, however, the electrical and mechanical properties of PPy have been assumed to be constant.

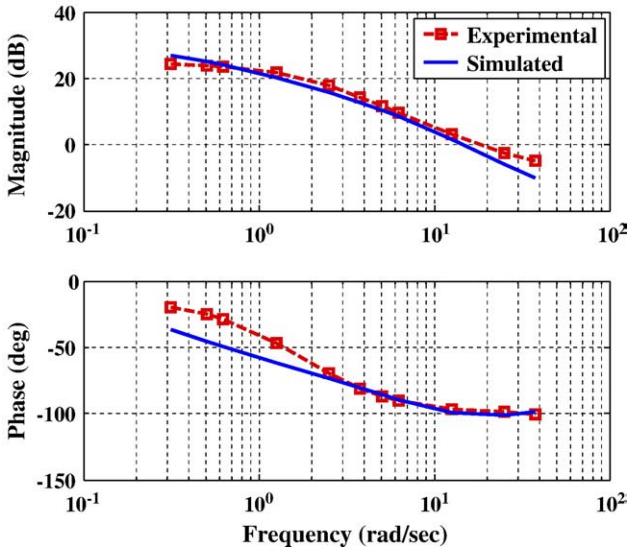

Fig. 16. Dynamic displacement response (size: 40×5 mm).

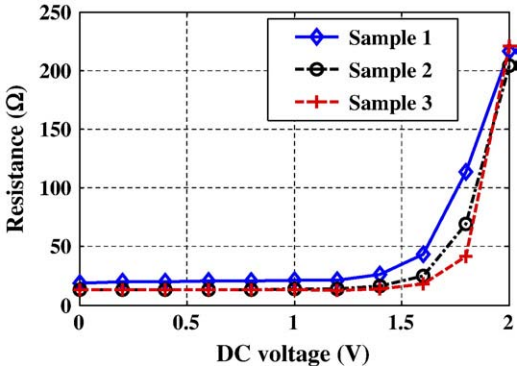

Fig. 17. Resistance of trilayer PPy actuator versus DC voltage (size: 15×3 mm).

This assumption is justified by that 1) the PPy is pre-doped and well-conducting [7], and 2) the magnitude of actuation voltage used is moderate for the purpose of scaling studies. These factors determine that the redox levels of both PPy layers stay within a limited range despite that when one layer is oxidized, the other layer would be reduced. Consequently, one can assume that electrical and mechanical properties of the trilayer actuator are nearly constant, and furthermore, the diffusive-elastic-metal model holds due to good conductivity of PPy layers throughout the actuation range used in this paper. Experimental results are further presented to support these statements.

In the first experiment the influence of the redox level on the resistance R is investigated. A DC voltage is applied to change the redox levels of both PPy layers. In the meantime a sinusoidal signal with frequency 250 Hz and amplitude 0.2 V is superimposed on the DC signal in order to measure the resistance of the actuator. A sequence of DC voltages is applied, from 0 V to 2 V, with steps of 0.2 V. Fig. 17 shows the variation of resistance with respect to the DC bias for three samples with identical dimensions (15×3 mm). It is clear that when the DC bias is below 1.5 V, the conductivity of the trilayer PPy actuator is high and consistent, which implies that both PPy layers are well conductive and the influence of redox level is negligible. When the DC voltage is above 1.5 V, the resistance increases significantly, which is consistent with the observations in literature [27].

The second experiment is an indirect measurement of the Young's modulus of PPy at different redox levels. The

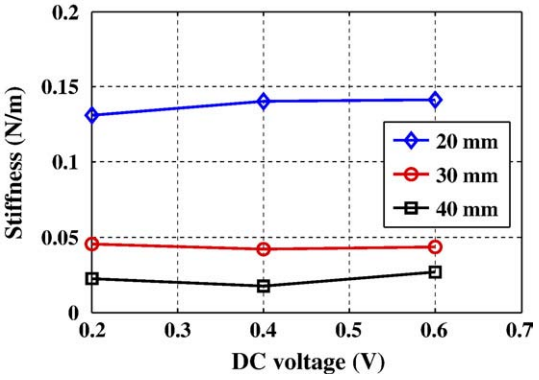

Fig. 18. Stiffness of trilayer PPy actuator versus DC voltage. The beams are 3.5 mm wide and have lengths of 20 mm, 30 mm, and 40 mm (with a 5 mm portion clamped).

experimental setup is the same as shown in Fig. 6. One can obtain the stiffness of a trilayer beam based on the slope of the measured force–displacement curve. Fig. 18 shows the stiffnesses of three beams under different DC actuation voltages, 0.2 V, 0.4 V, and 0.6 V. The stiffness showsmodest dependence on the DC voltage, but overall the correlation is insignificant, which implies that theimpact of redox level on the Young's modulus of Ppy can be ignored for the voltage range used.

6. Conclusions

In this paper a full electrochemomechanical model is presented for trilayer PPy actuators. The scaling laws for two important parameters, the double-layer capacitance and the resistance, are proposed and experimentally verified. The model can thus be written in terms of fundamental material parameters and actuator dimensions. Through experiments with actuators of different dimensions (length and width), the following aspects of the scalability of the model are independently validated: quasi-static force/displacement output, electrical admittance, and dynamic displacement response. In the future the scalability of the model in the thickness of PPy and PVDF layers will be experimentally examined.

The model will be instrumental in feasibility analysis for new applications of conjugated polymer actuators and in optimization of actuator fabrication and design. Although trilayer PPy actuators are used as an example throughout the paper, the work can be extended to other conjugated polymers with different configurations (bilayer or linear ones).

Since the paper is focused on the study of a scalable model, the PPy redox levels have been maintained in a moderate range so that nonlinearities, such as hysteresis and redox level-dependent properties, are not pronounced. For some applications, however, it can be desirable to extend the operation range of conjugated polymer actuators, in which case significant nonlinear behaviors might appear. It will then be of interest to incorporate these nonlinearities into the proposed model.

Acknowledgement

This research was supported in part by an NSF CAREER grant (ECS 0547131) and MSU IRGP (05-IRGP-418).

References

[1] Y. Bar-Cohen (Ed.), Electroactive Polymer (EAP) Actuators as Artificial Muscles: Reality, Potential, and Challenges, SPIE–The International Society for Optical Engineering, Bellingham, WA, 2001.
[2] E. Smela, Journal of Advanced Materials 15 (6) (2003) 481.
[3] M. Shahinpoor, K.J. Kim, Smart Materials and Structures 14 (2005) 197.
[4] Z. Chen, Y. Shen, N. Xi, X. Tan, Smart Materials and Structures 16 (2) (2007) S262.
[5] R. Baughman, Synthetic Metals 78 (1996) 339.
[6] G. Alici, B. Mui, C. Cook, Sensors and Actuators A 126 (2006) 396.
[7] Y. Wu, G. Alici, G.M. Spinks, G.G. Wallace, Synthetic Metals 156 (2006) 1017.
[8] A. Della Santa, D. De Rossi, A. Mazzoldi, Smart Materials and Structures 6 (1997) 23.
[9] A. Mazzoldi, D. De Rossi, in: Y. Bar-Cohen (Ed.), Smart Structures and Materials 2000: Electroactive Polymer Actuators and Devices, SPIE — The International Society for Optical Engineering, Bellingham, WA, 2000, p. 273.
[10] E.W.H. Jager, O. Inganas, I. Lunstrom, Science 288 (2000) 2335–2338.
[11] J. Zhou, H. Chan, T. To, K. Lai, W.J. Li, IEEE/ASME Transactions on Mechatronics 9 (2) (2004) 334.
[12] G. Alici, P. Metz, G.M. Spinks, Smart Materials and Structures 15 (2006) 243.
[13] G. Alici, N.N. Huynh, Sensors and Actuators A 132 (2) (2006) 616.
[14] M. Christophersen, B. Shapiro, E. Smela, Sensors and Actuators B 115 (2006) 596.
[15] J.D.W. Madden, Conducting polymer actuators, Phd thesis, MIT (2000).
[16] T. Amemiya, K. Hashimoto, A. Fujishima, Journal of Physical Chemistry 97 (1993) 4187.
[17] Y. Fang, X. Tan, G. Alici, Robust adaptive control of conjugated polymer actuators, IEEE Transactions on Control Systems Technology (in press).
[18] T.F. Otero, J.M. Sansinena, Bioelectrochemistry and Bioenergetics 42 (2) (1997) 117.
[19] P.G.A. Madden, Development and modeling of conducting polymer actuators and the fabrication of a conducting polymer based feedback loop, Phd thesis, MIT (2003).
[20] I. Ward, Mechanical Properties of Solid Polymers, Wiley, 1979.
[21] P. Magnusson, G. Alexander, V. Tripathi, A. Weisshaar, Transmission Lines and Wave Propagation, 4th Edition, CRC Press, 2001.
[22] G.F. Franklin, J.D. Powell, A. Emami-Naeini, Feedback Control of Dynamic Systems, 5th EditionPearson Education, Inc., Upper Saddle River, NJ, 2006.
[23] S. Satyanarayana, Surface stress and capacitive MEMS sensor arrays for chemical and biological sensing, Phd thesis, University of California, Berkeley (2005).
[24] Y. Shen, N. Xi, K.W.C. Lai, W.J. Li, Sensor Review 24 (2006) 274.
[25] C.O. Yoon, M. Reghu, D. Moses, A.J. Heeger, Physical Review B (Condensed Matter), 49 (1994) 10851.
[26] G. Spinks, L. Liu, G. Wallace, D. Zhou, Advanced Functional Materials 12 (2002) 437.
[27] D.L. Boxall, R.A. Osteryoung, Journal of The Electrochemical Society 151 (2) (2004) E41.